Hindawi Publishing Corporation
Journal of Nanomaterials
Volume 2015, Article ID 363175, 11 pages
http://dx.doi.org/10.1155/2015/363175

Research Article

Characterization and Evaluation of the Improved Performance of Modified Reverse Osmosis Membranes by Incorporation of Various Organic Modifiers and SnO_2 Nanoparticles

Kh. M. AL-Sheetan,[1] Mohammed Rafi Shaik,[2] A. S. AL-Hobaib,[1] and N. M. Alandis[2]

[1]*Nuclear Science Research Institute, King Abdulaziz City for Science and Technology (KACST), P.O. Box 6086, Riyadh 11442, Saudi Arabia*
[2]*Department of Chemistry, College of Sciences, King Saud University (KSU), P.O. Box 2455, Riyadh 11451, Saudi Arabia*

Correspondence should be addressed to A. S. AL-Hobaib; ahobaib@kacst.edu.sa

Received 11 March 2015; Revised 23 May 2015; Accepted 8 June 2015

Academic Editor: Vanna Torrisi

Reverse osmosis (RO) membranes modified with SnO_2 nanoparticles of varied concentrations (0.001–0.1 wt.%) were developed via in situ interfacial polymerization (IP) of trimesoyl chloride (TMC) and *m*-phenylenediamine (MPD) on nanoporous polysulfone supports. The nanoparticles dispersed in the dense nodular polyamide on the polysulfone side. The effects of IP reaction time and SnO_2 loading on membrane separation performance were studied. The modified reverse osmosis membranes were characterized by scanning electron microscopy (SEM), X-ray diffractometer (XRD), energy dispersive X-ray spectroscopy (EDX), transmission electron microscopy (TEM), contact angle measurement, and atomic force microscopy (AFM). The synthesized SnO_2 nanoparticles size varies between 10 and 30 nm. The results exhibited a smooth membrane surface and average surface roughness from 31 to 68 nm. Moreover, hydrophilicity was enhanced and contact angle decreased. The outcomes showed that an IP reaction time was essential to form a denser SnO_2-polyamide layer for higher salt rejection, the developed reverse osmosis membranes with the incorporation of the SnO_2 nanoparticles were examined by measuring permeate fluxes and salt rejection, and the permeate flux increased from 26 to 43.4 L/m^2·h, while salt rejection was high at 98% (2000 ppm NaCl solution at 225 psi (1.55 MPa), 25°C).

1. Introduction

The fresh water shortage is an increasingly vital challenge around the globe due to the speedy growth in population and the expanding prerequisites of agriculture and energy consumption along with pollution and shortages in water management [1]. Brackish water and seawater desalination can supply fresh water for irrigation, drinking, and industrial development. Among several desalination technologies, the membrane-based reverse osmosis (RO) process is easy to design and it has outstanding scale-up ability, and it presently controls the worldwide desalination market [2]. In the RO membrane desalination process, high performance semipermeable membranes play the most significant role because they govern the product quality of water and affect the whole energy consumption [3]. Therefore, high efficiency RO membranes with developed productivity along with better salt rejection are highly desired.

In 2012, 66 million m^3/d of drinkable water was generated through desalination; in 2015, this is estimated to reach 100 million m^3/d [4]. Reverse osmosis (RO) accounts for about 60% of world desalination capacity. Membranes, as the significant component of RO, regulate overall technical feasibility and economic efficiency.

Reverse osmosis (RO) membranes have been applied as a progressive water treatment process for the elimination of micropollutants and natural organic matter throughout the world. RO membranes are receiving the increased attention for a wide range of applications in water desalination, production of ultrapure water, and waste water treatment [5]. RO membranes developed via in situ interfacial polymerization (IP) of trimesoyl chloride (TMC) and *m*-phenylenediamine

(MPD) on nanoporous polysulfone supports [6]. Several polymers have been verified for their suitability in the development of thin film composite (TFC) reverse osmosis membrane [7, 8]. Owing to the outstanding separation performances including salt rejection and water flux, polyamide membranes are extensively recognized as the ideal among such RO membranes [9, 10].

In 1980s, first thin film composite (TFC) polyamide (PA) membranes were developed and are now the most extensively used desalination membranes due to the good stability over a wide range of pH values and high intrinsic water permeability [10, 11]. A characteristic thin film composite membrane is comprised of a porous, thick, nonselective layer along with an ultrathin sized barrier layer on its upper surface. This arrangement brings some significant advantages to the membranes. The thin film layer can be designed for the preferred combination of water flux and salt rejection; however, the porous support layer can be developed for decent mechanical properties combined with minimum resistance to permeate flow [10].

Nanotechnology offers a new method to develop performance of membrane by incorporating nanosized materials into the polyamide selective layer. Thin film nanocomposite (TFN) polyamide membrane containing zeolite nanosized material was first reported by Jeong et al.; subsequently other numerous nanomaterials, including silica [12, 13], silver [14], TiO_2 [15], and metal-organic frameworks [16], were verified, and most of the thin film nanocomposite membranes exhibited higher water permeate flux without decreasing salt rejection.

The suggested mechanisms of the enriched desalination performance of TFN membranes contain (i) faster passage of water within the porous nanomaterials [13]; (ii) improved membrane affinity to water [15, 17]; (iii) change in polyamide structure [12, 18, 19]. Nanomaterials may also improve some physical properties of membranes, such as mechanical strength and thermal stability.

Recent studies have revealed that mixed matrix membranes made by embedding porous materials in a polymeric matrix may considerably enhance membrane properties such as selectivity, surface area, permeability, stability, or catalytic activity in various membrane separation processes. Reverse osmosis (RO) thin film nanocomposite (TFN) membranes have been developed by incorporating pure metal, metal oxide, and tin nanoparticles into the polyamide layer [17, 18, 20, 21]. Precisely, the incorporation of SnO_2 in a PA layer has been established to improve its water permeability without significant loss of salt rejection under high pressure during RO process. However, the SnO_2-polyamide based thin film nanocomposite membranes were originally formulated for RO applications.

In this current study, SnO_2 nanoparticles were synthesized via Coprecipitation Method. The elemental composition and structure of the synthesized SnO_2 nanoparticles were characterized by X-ray powder diffraction (XRD), transmission electron microscope (TEM), and energy dispersive X-ray spectroscopy (EDX), respectively. The thin film nanocomposite membranes were synthesized by adding SnO_2 nanoparticles in amine solution in the interfacial polymerization (IP) method. Scanning electron microscopy (SEM) was subjected to examine the membrane morphology, isolated polyamide thin film layer, and distribution and dispersion of SnO_2 nanoparticles in polyamide. Deionized water contact angles were measured on air-dried samples of synthesized TFN membranes with different SnO_2 loadings to check the hydrophilicity of the membranes. The effects of IP reaction time and tin dioxide loading were evaluated by using 2000 ppm NaCl solution at 225 psi (1.55 MPa) and 25°C.

2. Experimental

2.1. Materials. Materials and chemical reagents which were used in this study are of analytical grade as shown below: sodium carbonate anhydrous (99%, Scharlau, Spain), polysulfone supports (PS-20, Sepro, USA), *m*-phenylenediamine (MPD) (99%, Sigma-Aldrich, USA), n-hexane (99%, Oxford Laboratory, India), n-dodecane (99%, Sigma-Aldrich, USA), n-cyclohexane (Scharlau, Spain), n-heptane (99%, Scharlau, Spain), 1,3,5-benzenetricarbonyl trichloride (TMC) (98%, Sigma-Aldrich, USA), Tin(II) chloride dehydrate (98%, BDH Chemicals Ltd. Poole, England), ammonium nitrate (AVONCHEM Limited, UK), and ultrapure deionized (DI) water from a Millipore Milli-Q system which was used in all experiments.

2.2. Methods

2.2.1. Preparation of SnO_2 Nanoparticles. The synthesis of SnO_2 nanoparticles (NPs) was conducted according to previously reported procedures [22]. 1.0 g $SnCl_2$ $4H_2O$ was dissolved in 50 mL distilled water, after which 5 mL ammonium solution (1.0 M) was mixed under vigorous stirring at ambient temperature. On addition of ammonia solution, light yellow color precipitate occurs. The achieved precipitate was centrifuged and washed several times with distilled water to remove any residual reactant (NH^{+4}, Cl^{-}) and to acquire neutral pH after which it was dried in oven at 60°C for 6 hours and collected sample was placed in furnace with the help of crucible under 300°C for 2 h.

2.2.2. Preparation of Polyamide Membranes. The polyamide (PA) thin film composite (TFC) membrane was synthesized by interfacial polymerization on PS20 support. The polysulfone support (PSF) was taped on a glass plate sensibly to avoid any probable penetration of liquid into its back from the sides. Then, it was soaked in deionized (DI) water for 1 min. At the end, the PSF support on the glass plate was taken out to eliminate the excess water on its top surface by standing vertically under ambient conditions. By immersing a polysulfone product support (PS-20) in an aqueous solution of *m*-phenylenediamine (MPD) (2% v/v) for 2 min, then the additional MPD solution was eliminated from the membrane by applying the pressure on membrane under rubber roller. The polyamide membrane was then immersed in 0.1% of benzene-1,3,5-tricarbonyl chloride (TMC) and hexane (99%) solution for 1 min, rinsed with 0.2% sodium carbonate, washed with deionized water, and finally stored in freezer at 4°C in deionized water until it was used.

2.2.3. Synthesis of Polyamide/SnO_2 Nanocomposite. SnO_2-polyamide nanocomposite membranes were prepared similarly to TFC membranes, except that SnO_2 nanoparticles were added in the 0.001–0.1 wt./v.% TMC in n-hexane solution beforehand. Varied amounts of SnO_2 nanoparticles (0.003, 0.005, and 0.08 wt./v.%) were dispersed in TMC-n-hexane solution by ultrasonicating for 30 min at 20°C. The resultant solution was immediately used for interfacial polymerization (IP) with MPD-soaked PS supports to form the TFN membranes.

2.3. Characterization and Instrumentation. The synthesized thin film nanocomposite (TFN) membrane morphology, elemental composition, and microstructure surface were investigated by using scanning electron microscopy (SEM) (FEI Nova-Nano SEM-600, Netherlands) and energy dispersive X-ray spectroscopy (EDX). The prepared SnO_2 nanoparticles were investigated for their size by using transmission electron microscopy (TEM) (JEM-2100F, JEOL, Japan). The membrane surface morphology roughness was studied by atomic force microscopy (AFM, Bruker Corporation). AFM images were produced by using Nanosurf scanning probe-optical microscope, small squares of the developed membranes (approximately 1 cm^2) were cut and pasted on glass substrate for the analysis, and average roughness of each sample was calculated.

Contact angle measurement was executed using a Ramé-Hart model 250 standard goniometer/tensiometer with drop image advanced software (Ramé-Hart Instrument Co., Succasunna, NJ 07876, USA). On the flat homogeneous dry membrane surface, a water droplet was located and the contact angle between the membrane and water was measured until no further variation was observed. The contact angle for average distilled water was determined in a series of 8 measurements for each of the different membrane surfaces. The performance of the developed nanocomposite membranes was analyzed through a cross-flow system (CF042SS316 Cell, Sterlitech Corp., USA). The valid membrane area in this system was 42 cm^2. The feed water temperature was 25°C with pH adjusted between 6 and 7, 2000 ppm feed NaCl, and 1 gallon per minute (gpm) feed flow rate. The filtration process was carried out at the pressure of 225 psi. All measurements of the water flux and salt rejection were carried after 30 min of water filtration experiments to confirm that had reached stability. Figure 1 shows the representation diagram of the cross-flow filtration system.

The water flux was determined according to the following equation [23]:

$$J = \frac{V_p}{A * t}, \quad (1)$$

where J is the water flux (L/m^2 h), V_p is the permeate volume (L), A is the area of the membrane (m^2), and t is the treatment time (h). The salt rejection (R) was achieved using the following equation:

$$R = \left(1 - \frac{C_p}{C_f}\right) * 100, \quad (2)$$

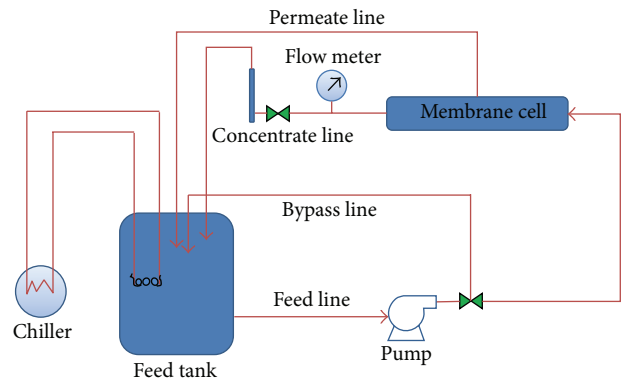

Figure 1: Schematic illustration of forward cross-flow filtration system.

where C_p and C_f are the salt concentrations of permeate and feed, respectively.

3. Results and Discussion

3.1. Characterization of the Synthesized SnO_2 Nanoparticles. The synthesized SnO_2 nanoparticles were characterized by four different instrumental methods such as SEM (scanning electron microscope), TEM (transmission electron microscopy), EDX (energy dispersive X-ray spectroscopy), and XRD (X-ray diffraction) as follows.

3.1.1. SEM and EDX Analysis of SnO_2 Nanoparticles. SnO_2 nanoparticles size and surface morphology were examined by scanning electron microscopic analysis (SEM), as shown in Figure 2(b). Figure 2(b) shows lots of ridge and valley structures and considerably smaller protuberances structures adjacent to the ridges. Energy dispersive X-ray spectroscopy (EDX) carried out during the SEM analysis conforms to the characteristic peaks of Sn, as shown in Figure 2(a). The atomic ratio between oxygen and tin was calculated using EDX graph and the obtained ratio of Sn and O atom was found to be 1 : 1.60. So the atomic ratio Sn : O was approximately 1 : 2, which indicates that the tin oxide is compositional.

3.1.2. TEM Analysis of SnO_2 Nanoparticles. The TEM analysis was carried out by accelerating voltage in the range of 20–200 kV with 2.4 Å resolution by dispersion SnO_2 in ethanol with ultrasonic wave for one hour. After sonication sample was deposited on Cu grid and observed at high magnification, the size of SnO_2 nanoparticles was observed in the range of 10 to 30 nm. TEM images are shown in Figure 3.

3.1.3. XRD Analysis of SnO_2 Nanoparticles. Then, the crystal structure of SnO_2 nanoparticles was characterized by XRD. The results are shown in Figure 4. The XRD results pattern shows that SnO_2 nanoparticles are well crystalline and reveals all diffraction peaks, and the average grain size was calculated using the Debye-Scherrer equation ($G = 0.9\lambda/\beta\cos\theta$), where λ is the X-ray wavelength (Cu, 1. 5418 Å), θ is the maximum of the Bragg diffraction peak, and β is the full width at

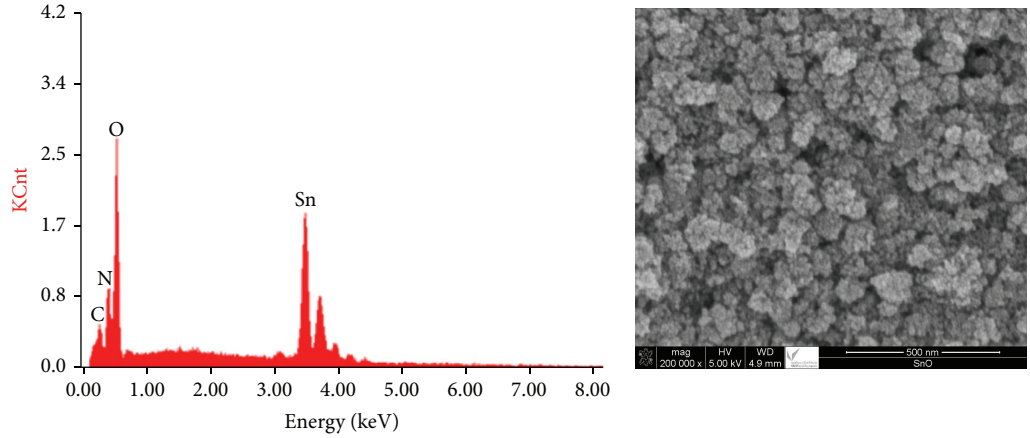

(a) EDX of graph (b) SEM of SnO_2 nanoparticles

FIGURE 2: SEM and EDX of SnO_2 nanoparticles.

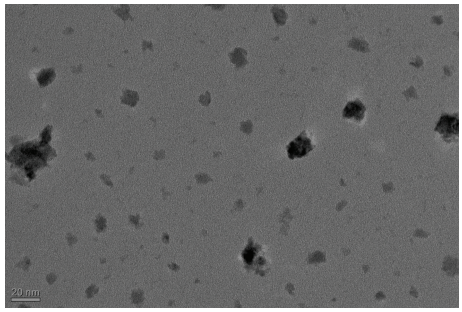

FIGURE 3: TEM image of SnO_2 nanoparticles.

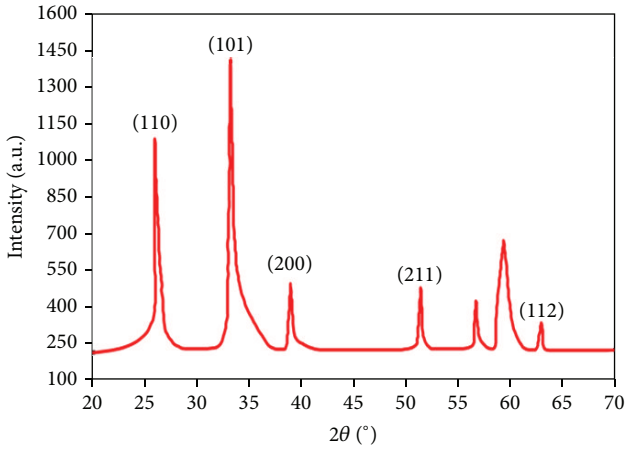

FIGURE 4: XRD patterns of SnO_2 nanoparticles.

half-maximum. The diffraction peaks resemble the tetragonal rutile SnO_2 nanostructure with values of lattice constants $a = 0.4750$ nm and $c = 0.3185$ nm. It can be noticed that the reflection is significantly broadened, demonstrating that average crystalline size of SnO_2 nanoparticle is 30 nm. It can be noticed that the reflection is significantly broadened and the average size of the nanoparticle calculated using the Debye-Scherrer equation demonstrated that the average crystalline size of SnO_2 nanoparticle is approximately 30 nm.

3.2. Characterizations of Modified Membranes with SnO_2 Nanoparticles. The polyamide membrane established in the presence of tin dioxide nanoparticles was characterized to investigate the surface morphology, contact angle, water permeate flux, and salt rejection capability by using various instrumental techniques as described below.

3.2.1. SEM with EDX Analysis. The surface morphology of thin film composite membranes was examined by using SEM to investigate the effects of tin dioxide incorporation. The SEM images of the top surface of TFC and TFN (0.003 and 0.005 wt.% tin dioxide loading) membranes are displayed in Figure 5, which is the typical polyamide membrane morphology developed through interfacial polymerization of MPD and TMC. The tin dioxide nanoparticles incorporation did not affect the overall morphology of the polyamide thin film layer. Nevertheless, a few cubic-like structures could be observed on the surface of TFN membrane, which was in reliable with the morphology of tin dioxide nanoparticles. EDX spectra and SEM images of the reference TFC membrane are displayed in Figures 5(a) and 5(b), respectively. Similarly, EDX spectra and SEM images of polymer membranes containing tin nanoparticles are shown in Figures 5(c) and 5(d), respectively. It was noticed that the incorporation of SnO_2 nanoparticles in the polymer matrix does not show much effect on the overall morphology of TFC membrane containing tin nanoparticles, even though the wt.% range of SnO_2 nanoparticles was increased up to 0.08 wt.% (see Figure 5(h)). However, SnO_2 nanoparticles partial aggregation was observed in the polymer matrix. The difference between the images shows clearly the presence of SnO_2 nanoparticles. This was further proved by EDX quantitative analysis which shows clearly the presence of carbon, oxygen, and tin peaks as component elements. Comprehensive

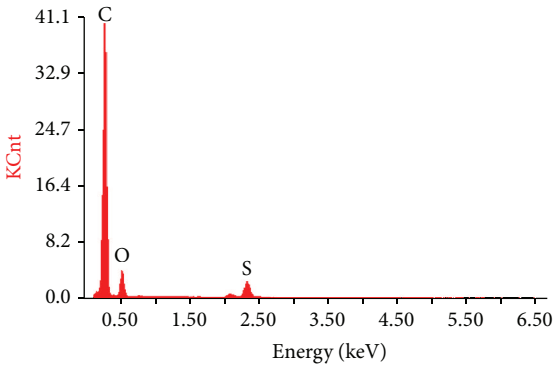

(a) EDX of TFC reference

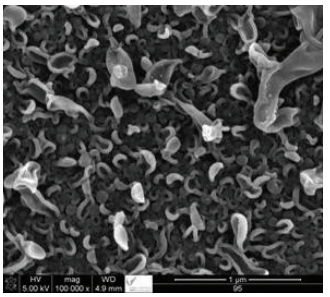

(b) SEM of TFC reference

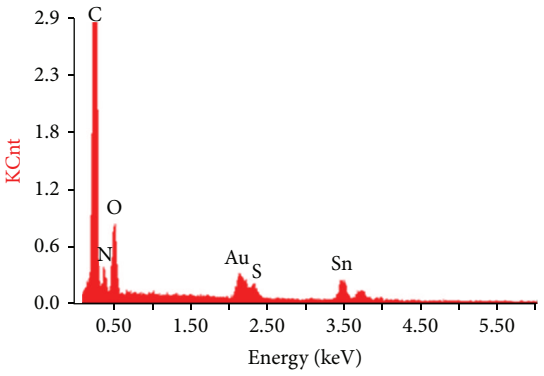

(c) EDX of modified membrane (0.003 wt.%)

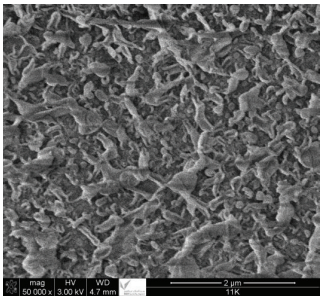

(d) SEM of modified membrane (0.003 wt.%)

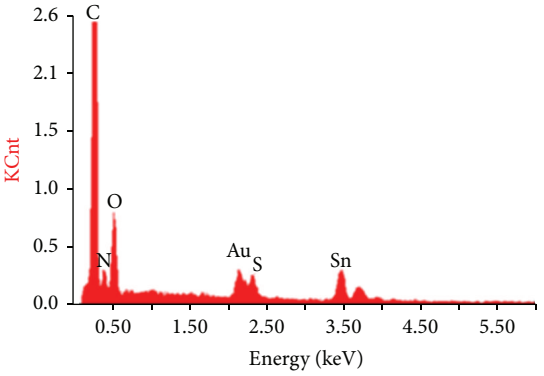

(e) EDX of modified membrane (0.005 wt.%)

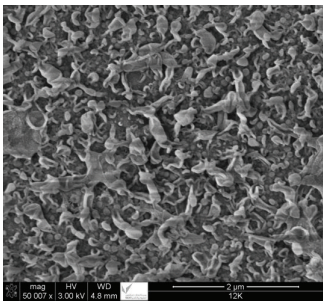

(f) SEM of modified membrane (0.005 wt.%)

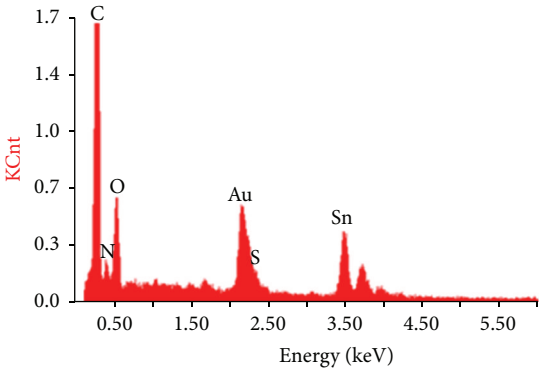

(g) EDX of modified membrane (0.08 wt.%)

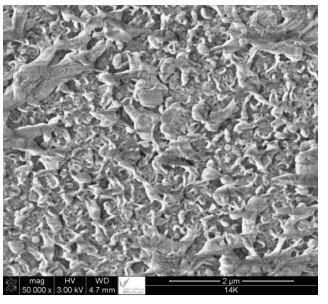

(h) SEM of modified membrane (0.08 wt.%)

Figure 5: SEM and EDX of TFC reference and modified membrane with SnO_2 nanoparticles.

observation demonstrates that the ridge-valley structure of active layer on TFC membrane presented a comparative flat surface, as shown in Figure 5(a). In comparison, TFN membranes display ascendant and broaden ridge-valley structure, which recommend variation on surface roughness of TFN membranes under different nano-SnO_2 loadings.

3.2.2. AFM Results. The synthesized polymer nanocomposite membranes surface morphology and roughness were investigated by atomic force microscope (AFM). AFM micrograms were taken for membranes containing different contents of tin dioxide nanoparticles and are shown in Figure 6. It is observed that the roughness (Ra) values increased with increase in tin dioxide content in the polymer membranes. TFC membranes with 0.08 wt.% tin dioxide exhibit the highest surface roughness (i.e., Ra = 68 nm), compared to that (Ra = 31 nm) of TFC reference membrane without any tin content. This difference is supposed to be caused by the leaf-like shape as well as by the aggregation of SnO_2 nanoparticles existing in the membrane surface.

3.2.3. Contact Angle Measurements. Polyamide/SnO_2 nanocomposite membranes were directed to contact angle measurements in order to estimate the hydrophilic and hydrophobic characters of the membranes. During contact angle measurements, reproducible standard deviation (SD) was taken into account. The contact angle measurement of various amounts (wt.%) of tin dioxide polymer nanocomposite membranes is shown in Figure 7.

It is noticed that contact angle substantially decreases with increase of SnO_2 content in the membranes. For example, 0.06 wt.% SnO_2 membrane shows that the contact angle drops from 94° to 15° and it is also revealed that after 0.08 wt.% SnO_2 loaded membranes show no change or decrease in contact angle. On the other hand, the nanocomposite polyamide membrane has higher hydrophilicity which is considered a significant property of membranes, as it affects their flux properties. Consequently, the presence of hydrophilic tin nanoparticles in membrane structures can increase the hydrophilicity of membrane because a larger fraction of water diffuses through the membrane structure.

It is eminent that there is a strong correspondence between the orientation (geometry) of water at a solid-liquid interface and the hydrophilicity of the solid surface [24, 25]. Rearrangement of interfacial water molecules can also describe the cause of increased hydrophilicity. The interfacial water molecules increased rearrangement may progress the water molecule's capability to form hydrogen bonds and in turn can create stronger interactions between solid phase and water in polymer matrix that is thin film composite surface.

Significant decrease of contact angles in the existence of embedded tin dioxide nanoparticles can be described as follows. The hydrophilic character of the membrane surface increases due to the large amount of embedded spherical shaped SnO_2 nanoparticles hydrophobic nature exposed on the membrane surface. Furthermore, the membrane surface could even become of more hydrophilic nature due to the capability of the hydrophilic pores to absorb water via capillary effects [26]. This is reliable with the result of Jeong et al. [17], who noticed that the membrane surface contact angle decreased with increased concentration of zeolite and attributed this to the super-hydrophilic property of zeolite.

Tin dioxide nanoparticles contacting with MPD aqueous solution may become hydrated and release heat [18]. This method may interfere in the interfacial polymerization reaction between TMC and MPD and subsequently affect the chemical structure of the PS support. If enormous number of acyl chloride groups of TMC remained on the membrane surface without reacting with amine groups of MPD, the hydrolysis of acyl chloride could produce carboxylic acid functional groups leading to increased hydrophilicity [27], thereby generating favorable conditions for improved water flux and antifouling ability. It is understood that morphological structure and hydrophilicity of the membrane are the two key factors that manage the filtration properties of thin film composite membrane [28].

3.3. RO Membrane Performance

3.3.1. Water Flux and Salt Rejection. The filtration process of various amounts of SnO_2 nanoparticles loaded polymer membranes was carried out at 25°C by using cross-flow method. Results of water permeate fluxes and salt rejection of all these polymer nanocomposite membranes are presented in Figure 8.

Most of the hybrid membranes water fluxes are higher than that of the TFC membranes (26 L/m^2 h ± 2.2), where ±2.2 was the SD of three measurements which was used to calculate the uncertainty of these measurements. The amount of SnO_2 nanoparticles was increased and then the water flux of the membrane also increased up to a peak value at 0.005 wt.% (43.4 L/m^2 h ± 3.1) and then started to decrease. The peak value of water flux shows an improvement of 167% over that of the TFC reference membrane. On the other hand, the salt rejection of both TFC and TFN membranes was found to be 98% ± 0.2 and 99% ± 0.3, respectively. The SD was calculated for three measurements in each case. Therefore, the deviation of salt rejection for TFN was within 2%. It is hypothesized that the enriched water permeability may be attributed to the subnanometer pores in the tin dioxide nanoparticles. Alternatively, the tin nanoparticles may affect the interfacial polymerization process to modify the active layer permeability. Moreover, the increased membrane surface roughness (and thus increased surface area of polyamide) might partially describe such water flux enhancement. On the other hand, a high tin loading may help to form a relatively thicker polyamide rejection layer, which decreased the water permeability and enhanced salt rejection.

3.3.2. Optimization of MPD and TMC. Water flux and salt rejection both depend on the density of the polyamide layer, which is effected by, for example, crosslink density [29]. The density of the polymer across the barrier layer is not uniform [30]. The core layer is the densest region and the density of polymer decreases step by step as the polymer expands further into the organic phase [31, 32].

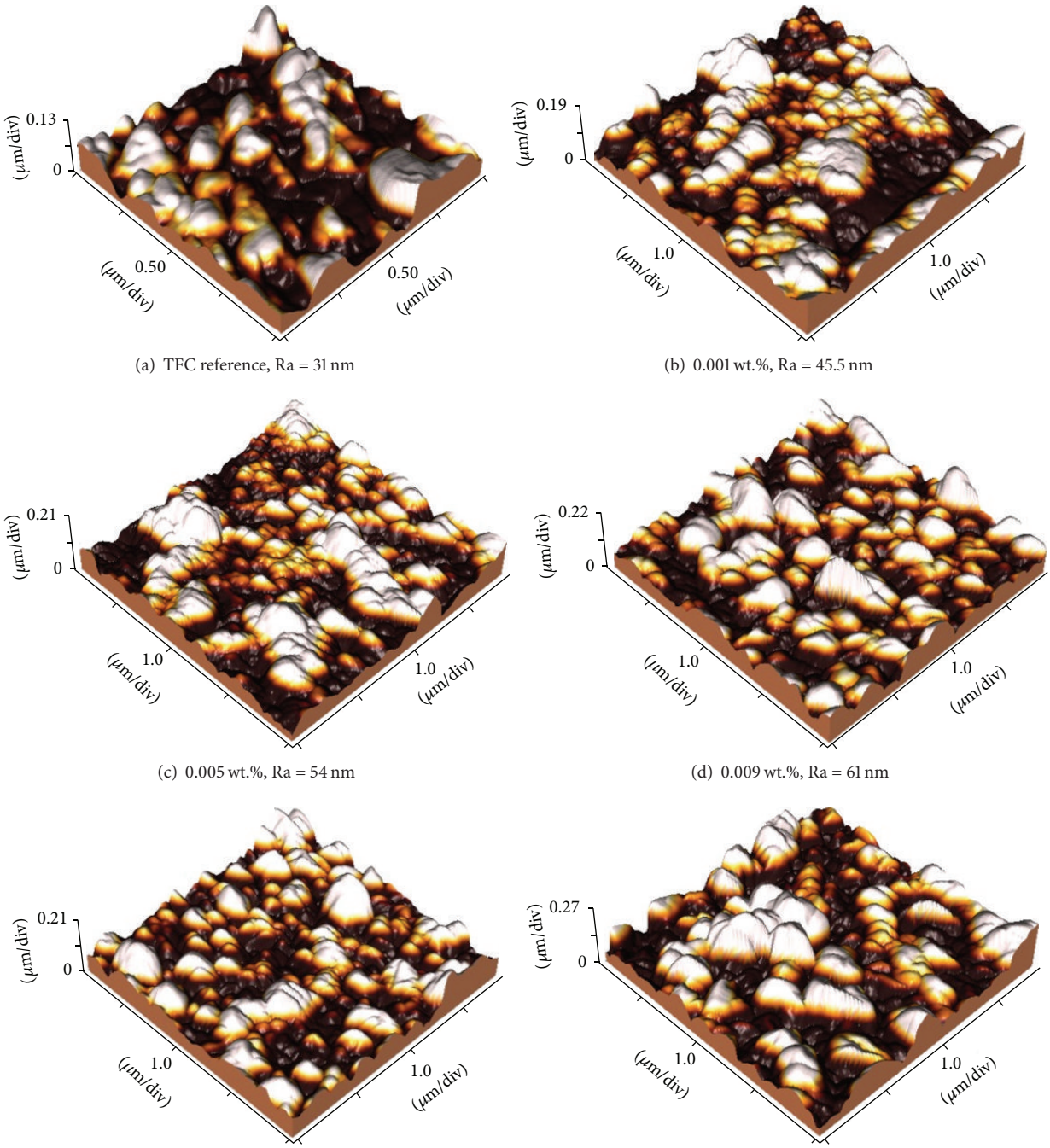

(a) TFC reference, Ra = 31 nm

(b) 0.001 wt.%, Ra = 45.5 nm

(c) 0.005 wt.%, Ra = 54 nm

(d) 0.009 wt.%, Ra = 61 nm

(e) 0.02 wt.%, Ra = 65 nm

(f) 0.08 wt.%, Ra = 68 nm

Figure 6: AFM images of modified membrane with SnO_2 nanoparticles.

In numerous applications using MPD and TMC in interfacial polymerization, in this IP process the initial concentration of amine is much higher than the concentration of acyl chloride. Whether the concentration of acyl chloride is increased or the concentration of amine is decreased, it results in a denser polyamide layer, related to those developed using higher amine/acyl chloride molar ratios [33]. Increases in either the thickness or density of the barrier layer (TMC/MPD) should increase the mass transfer resistance of the resulting membrane, thereby reducing permeate flux. By altering monomers, initial concentration can affect the membrane's water and salt passage properties.

The modified thin film composite membranes were synthesized by varying the concentration of MPD and TMC and keeping the mass of added SnO_2 nanoparticles at 0.005 wt.%. Figure 9 exhibits results of the influence of variation of

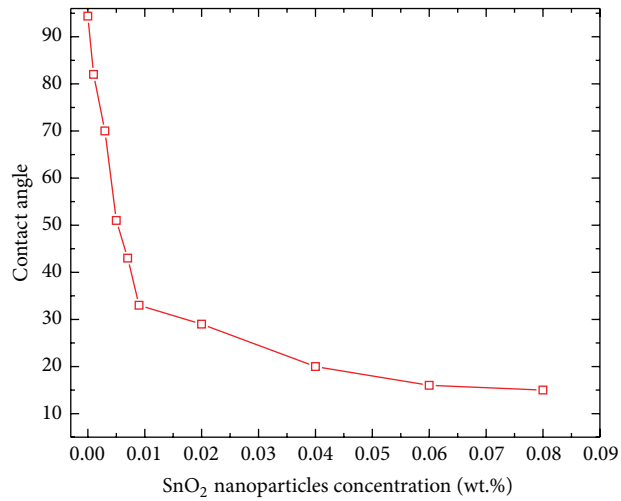

Figure 7: Contact angles of PA membranes with different amounts of SnO_2 nanoparticles.

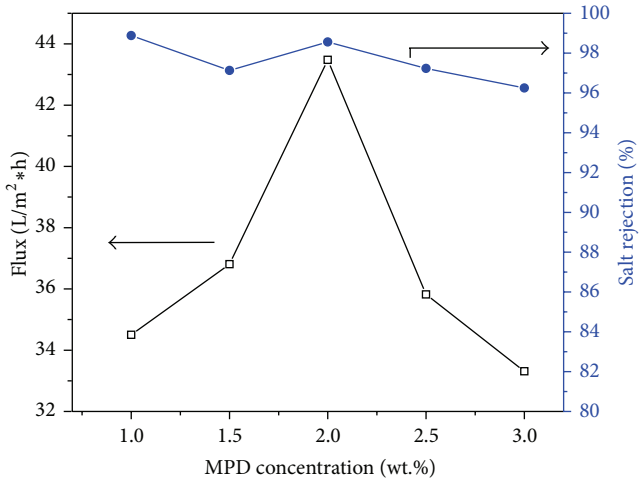

Figure 9: Water permeate flux and salt rejection of modified membranes containing fixed amounts of SnO_2 nanoparticles at 0.005 wt.% and TMC at 0.1 w/v.%.

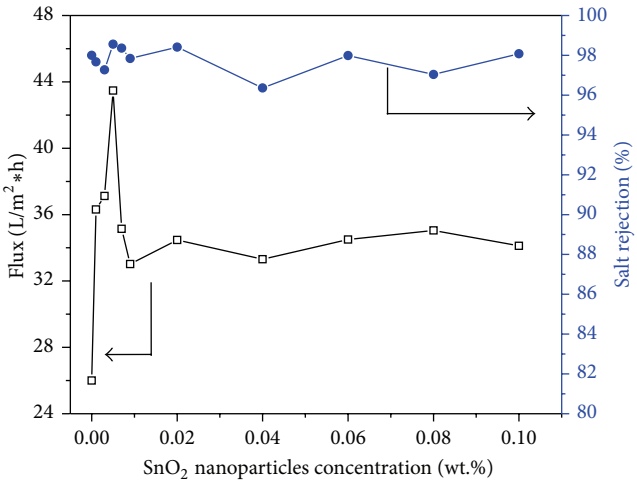

Figure 8: Water permeate flux and salt rejection of modified membrane containing various amounts of SnO_2 nanoparticles.

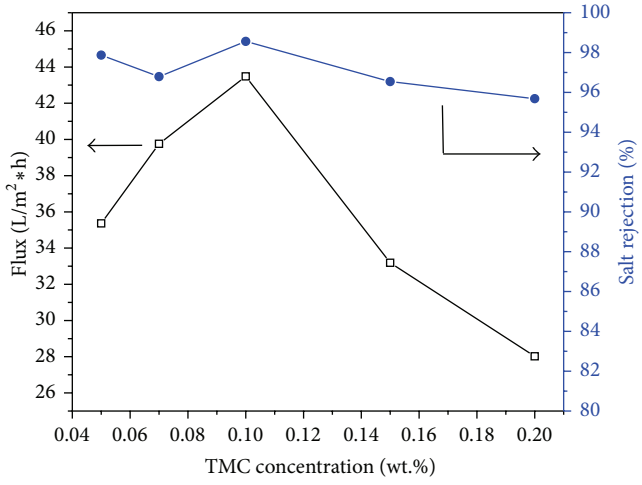

Figure 10: Water permeate flux and salt rejection of modified membranes containing fixed amounts of SnO_2 nanoparticles at 0.005 wt.% and MPD at 2 w/v.%.

MPD concentration on permeate flux and salt passage. Correspondingly, Figure 10 shows influence of change of TMC concentration on permeates flux and salt rejection.

The salt passage was found to be relatively insensitive to change of MPD concentration, signifying the establishment of defect-free membranes in all cases. High permeate flux was observed near 2% (w/v) MPD. As concentration of MPD was increased, the driving force for MPD diffusion into the organic phase increased. The concentration of MPD increases which would tend to increase the thickness of the barrier layer and it causes lower permeate flux. As concentration of MPD decreases, layer thickness is also expected to decrease; in this circumstance, permeate flux increases but the molar ratio of $-NH_2$ and $-COCl$ becomes closer to unite the resulting polyamide layer expected to become denser, which would lower water permeate flux [31, 34].

Figure 10 demonstrates the concentration of TMC influence in the organic phase on water permeate flux and salt passage at a constant MPD concentration of 2 w/v.% in the aqueous phase, which was noticed in Figure 9 to be near the optimum flux value. Since IP is typically MPD diffusion controlled during growth of the polyamide layer, the SnO_2 nanoparticles might provide a mass transfer resistance to the MPD diffusion across the interface and affect the reaction of amine and acyl chloride groups, which could result in a moderately looser structure of the thin film layer. Variations in TMC concentration would influence the layer density by changing the amine/acyl chloride molar ratio [31, 34]. As TMC concentration increases, the amine/acyl chloride molar ratio decreases, which is predicted to increase film density, resulting in lower permeate flux [31, 34]. Although a decrease in permeate flux was also noticed at the lowest

Table 1: Showing summary of previous studies.

Nanoparticles type	Method	Measuring conditions	Modified membrane properties	Salt rejection	Flux L/m^2h	Ref.
Silica nanoparticles	IP (MPD/TMC). Silica in MPD/water.	NaCl aqueous solution of 2000 ppm, pressures of 250 psig.	Tunable pore radius and higher thermal stability.	71.7	40.8	[12]
Silver nanoparticles	IP (MPD/BTC). Silica in BTC.	2000 ppm aqueous $MgSO_4$ solution, pressures of 250 psig.	Higher antibiofouling effect.	97	94	[14]
TiO_2 nanoparticles	IP (MPD/TMC). TiO_2 in TMC and HCFC.	2000 ppm $MgSO_4$ solution at a pressure of 0.2–1 MPa and 25°C.	Enhanced surface hydrophilicity.	95	9.1	[15]
Zeolite nanoparticles	IP (MPD/TMC). NaY in TMC/hexane.	2000 ppm solutions of (a) NaCl, (b) $MgSO_4$, and (c) PEG200; pressure of 1.55 MPa.	Increased roughness and contact angle.	90.5	43.7	[18]
Zeolite nanoparticles	IP (MPD/TMC). NaA in TMC/hexane.	2000 ppm NaCl solution at 25°C; pressure of 1.6 MPa.	Smoother, hydrophilic and negatively charged surfaces.	93	40.2	[19]
Silica nanoparticles	IP (MPD/TMC). Silica in MPD/water.	500 ppm dioxane; pressure 50–200 psig.	Silica particle interacting well with the polyamide.	91	27.2	[36]
TiO_2 nanoparticles	The neat TFC membrane was dipped in the transparent TiO_2 colloidal solution.	2000 ppm NaCl solution at 25°C; pressure 225 psi.	Higher photocatalytic bactericidal efficiency under UV light.	96.6	24.5	[37]
Al_2O_3 nanoparticles	IP (MPD/TMC). Al_2O_3 in TMC/hexane.	NaCl aqueous solutions of 1000 ppm, pressure of 1 MPa, and a temperature of 25°C.	Enhanced surface hydrophilicity.	88	5	[39]

TMC concentration considered, at low TMC concentration (<0.1%), the IP reaction is reported to be TMC diffusion limited [35]. Acyl chloride groups low concentration in the reaction zone may permit the polyamide film to grow thicker, which would decrease flux [29].

3.3.3. Alternative Solvents. The abovementioned experiments were carried out in hexane medium, n-cyclohexane, and n-heptane, and n-dodecane solvents were used in place of hexane to monitor influence of change of solvent on flux and salt rejection. Figures 11 and 12 compile the results of flux and the results are in the order of n-dodecane > n-heptanes > n-cyclohexane > n-hexane. However, the slat rejection result altered within 2%.

3.4. Summary of Modified RO Membranes Properties of Previous Studies. There are numerous literature reports concerning the performance of interfacial polymerized commercial polyamide of TFC membranes and aromatic polyamide and desalination of TFC membranes depend on MPD and TMC [12, 14, 15, 17–19, 36–39]. The transport properties of the membranes prepared in this work were found comparable to those of the membranes reported in Table 1.

4. Conclusions

SnO_2 nanoparticles were prepared via coprecipitation method and characterized by different characterization tools such as energy dispersive X-ray spectroscopy, transmission electron microscopy, and X-ray diffractometer. The synthesized SnO_2 nanoparticles were embedded into polyamide membrane through interfacial polymerization method. Scanning electron microscopy confirms the formation of polyamide membrane embedded with tin dioxide nanoparticles. EDX quantitative analysis confirms the presence of tin dioxide-polyamide components. The performance on water flux and salt rejection revealed that the performance of nanocomposite membrane was better than the pristine membrane. Moreover, the permeate flux was improved

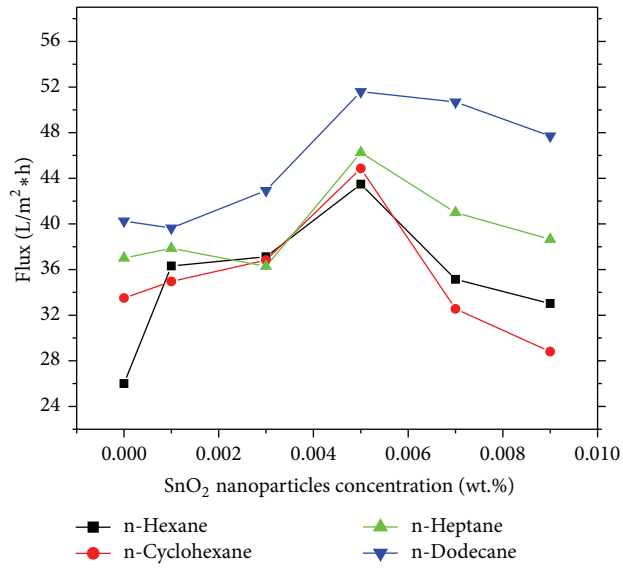

Figure 11: Water fluxes with different solvents.

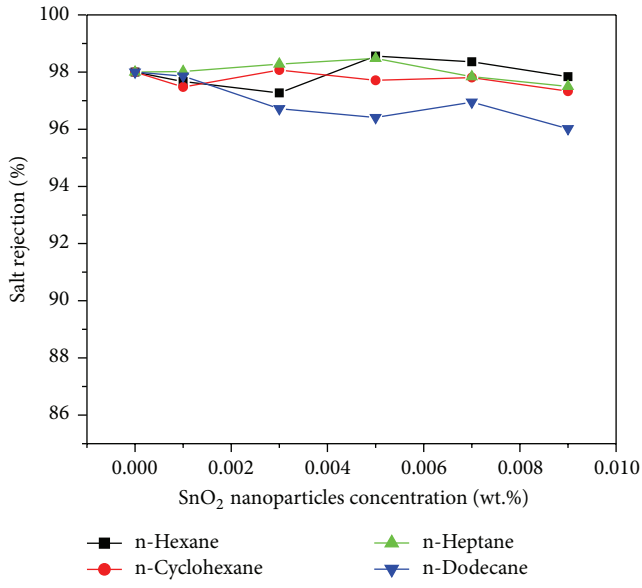

Figure 12: Salt rejection with different solvents.

(26 to 43.4 L/m^2·h), with slight change of salts rejection result within 2%.

Conflict of Interests

The authors declare that there is no conflict of interests regarding the publication of this paper.

Acknowledgments

The authors are grateful to King Abdulaziz City for Science and Technology, Riyadh, Saudi Arabia, for the financial support of this work and the facilities in its labs. This work was supported by King Saud University, Deanship of Scientific Research, College of Science, Research Center.

References

[1] M. A. Eltawil, Z. Zhengming, and L. Yuan, "A review of renewable energy technologies integrated with desalination systems," *Renewable and Sustainable Energy Reviews*, vol. 13, no. 9, pp. 2245–2262, 2009.

[2] B. L. Pangarkar, M. G. Sane, S. B. Parjane, and M. Guddad, "Status of membrane distillation for water and wastewater treatment—a review," *Desalination and Water Treatment*, vol. 52, no. 28–30, pp. 5199–5218, 2014.

[3] M. A. Shannon, P. W. Bohn, M. Elimelech, J. G. Georgiadis, B. J. Marīas, and A. M. Mayes, "Science and technology for water purification in the coming decades," *Nature*, vol. 452, no. 7185, pp. 301–310, 2008.

[4] L. F. Greenlee, D. F. Lawler, B. D. Freeman, B. Marrot, and P. Moulin, "Reverse osmosis desalination: water sources, technology, and today's challenges," *Water Research*, vol. 43, no. 9, pp. 2317–2348, 2009.

[5] V. K. Gupta, I. Ali, T. A. Saleh, A. Nayak, and S. Agarwal, "Chemical treatment technologies for waste-water recycling—an overview," *RSC Advances*, vol. 2, no. 16, pp. 6380–6388, 2012.

[6] M. Elimelech and W. A. Phillip, "The future of seawater desalination: energy, technology, and the environment," *Science*, vol. 333, no. 6043, pp. 712–717, 2011.

[7] K. P. Lee, T. C. Arnot, and D. Mattia, "A review of reverse osmosis membrane materials for desalination—development to date and future potential," *Journal of Membrane Science*, vol. 370, no. 1, pp. 1–22, 2011.

[8] L. Shi, S. R. Chou, R. Wang, W. X. Fang, C. Y. Tang, and A. G. Fane, "Effect of substrate structure on the performance of thin-film composite forward osmosis hollow fiber membranes," *Journal of Membrane Science*, vol. 382, no. 1-2, pp. 116–123, 2011.

[9] S. Mondal and S. R. Wickramasinghe, "Produced water treatment by nanofiltration and reverse osmosis membranes," *Journal of Membrane Science*, vol. 322, no. 1, pp. 162–170, 2008.

[10] J. E. Cadotte, "Interfacially synthesized reverse osmosis membrane," Ed., Google Patents, 1981.

[11] R. E. Larson, J. E. Cadotte, and R. J. Petersen, "The FT-30 seawater reverse osmosis membrane—element test results," *Desalination*, vol. 38, pp. 473–483, 1981.

[12] G. L. Jadav and P. S. Singh, "Synthesis of novel silica-polyamide nanocomposite membrane with enhanced properties," *Journal of Membrane Science*, vol. 328, no. 1-2, pp. 257–267, 2009.

[13] J. Yin, E.-S. Kim, J. Yang, and B. Deng, "Fabrication of a novel thin-film nanocomposite (TFN) membrane containing MCM-41 silica nanoparticles (NPs) for water purification," *Journal of Membrane Science*, vol. 423-424, pp. 238–246, 2012.

[14] S. Y. Lee, H. J. Kim, R. Patel, S. J. Im, J. H. Kim, and B. R. Min, "Silver nanoparticles immobilized on thin film composite polyamide membrane: characterization, nanofiltration, antifouling properties," *Polymers for Advanced Technologies*, vol. 18, no. 7, pp. 562–568, 2007.

[15] H. S. Lee, S. J. Im, J. H. Kim, H. J. Kim, J. P. Kim, and B. R. Min, "Polyamide thin-film nanofiltration membranes containing TiO_2 nanoparticles," *Desalination*, vol. 219, no. 1, pp. 48–56, 2008.

[16] S. Sorribas, P. Gorgojo, C. Téllez, J. Coronas, and A. G. Livingston, "High flux thin film nanocomposite membranes based

on metal–organic frameworks for organic solvent nanofiltration," *Journal of the American Chemical Society*, vol. 135, no. 40, pp. 15201–15208, 2013.

[17] B.-H. Jeong, E. M. V. Hoek, Y. Yan et al., "Interfacial polymerization of thin film nanocomposites: a new concept for reverse osmosis membranes," *Journal of Membrane Science*, vol. 294, no. 1-2, pp. 1–7, 2007.

[18] M. L. Lind, A. K. Ghosh, A. Jawor et al., "Influence of zeolite crystal size on zeolite-polyamide thin film nanocomposite membranes," *Langmuir*, vol. 25, no. 17, pp. 10139–10145, 2009.

[19] H. Huang, X. Qu, H. Dong, L. Zhang, and H. Chen, "Role of NaA zeolites in the interfacial polymerization process towards a polyamide nanocomposite reverse osmosis membrane," *RSC Advances*, vol. 3, no. 22, pp. 8203–8207, 2013.

[20] S. H. Kim, S.-Y. Kwak, B.-H. Sohn, and T. H. Park, "Design of TiO_2 nanoparticle self-assembled aromatic polyamide thin-film-composite (TFC) membrane as an approach to solve biofouling problem," *Journal of Membrane Science*, vol. 211, no. 1, pp. 157–165, 2003.

[21] M. L. Lind, D. E. Suk, T.-V. Nguyen, and E. M. V. Hoek, "Tailoring the structure of thin film nanocomposite membranes to achieve seawater RO membrane performance," *Environmental Science & Technology*, vol. 44, no. 21, pp. 8230–8235, 2010.

[22] M. Alam, A. A. Ansari, M. R. Shaik, and N. M. Alandis, "Optical and electrical conducting properties of Polyaniline/Tin oxide nanocomposite," *Arabian Journal of Chemistry*, vol. 6, no. 3, pp. 341–345, 2013.

[23] M. L. Lind, D. E. Suk, T.-V. Nguyen, and E. M. V. Hoek, "Tailoring the structure of thin film nanocomposite membranes to achieve seawater RO membrane performance," *Environmental Science and Technology*, vol. 44, no. 21, pp. 8230–8235, 2010.

[24] G. Hurwitz, G. R. Guillen, and E. M. V. Hoek, "Probing polyamide membrane surface charge, zeta potential, wettability, and hydrophilicity with contact angle measurements," *Journal of Membrane Science*, vol. 349, no. 1-2, pp. 349–357, 2010.

[25] Q. Du, E. Freysz, and Y. R. Shen, "Surface vibrational spectroscopic studies of hydrogen bonding and hydrophobicity," *Science*, vol. 264, no. 5160, pp. 826–828, 1994.

[26] J.-H. Li, Y.-Y. Xu, L.-P. Zhu, J.-H. Wang, and C.-H. Du, "Fabrication and characterization of a novel TiO_2 nanoparticle self-assembly membrane with improved fouling resistance," *Journal of Membrane Science*, vol. 326, no. 2, pp. 659–666, 2009.

[27] C. K. Kim, J. H. Kim, I. J. Roh, and J. J. Kim, "The changes of membrane performance with polyamide molecular structure in the reverse osmosis process," *Journal of Membrane Science*, vol. 165, no. 2, pp. 189–199, 2000.

[28] H. Wu, B. Tang, and P. Wu, "Novel ultrafiltration membranes prepared from a multi-walled carbon nanotubes/polymer composite," *Journal of Membrane Science*, vol. 362, no. 1-2, pp. 374–383, 2010.

[29] Y. Song, P. Sun, L. L. Henry, and B. Sun, "Mechanisms of structure and performance controlled thin film composite membrane formation via interfacial polymerization process," *Journal of Membrane Science*, vol. 251, no. 1-2, pp. 67–79, 2005.

[30] G. E. Mitchell, B. Mickols, D. Hernandez-Cruz, and A. Hitchcock, "Unexpected new phase detected in FT30 type reverse osmosis membranes using scanning transmission X-ray microscopy," *Polymer*, vol. 52, no. 18, pp. 3956–3962, 2011.

[31] V. Freger, "Nanoscale heterogeneity of polyamide membranes formed by interfacial polymerization," *Langmuir*, vol. 19, no. 11, pp. 4791–4797, 2003.

[32] F. A. Pacheco, I. Pinnau, M. Reinhard, and J. O. Leckie, "Characterization of isolated polyamide thin films of RO and NF membranes using novel TEM techniques," *Journal of Membrane Science*, vol. 358, no. 1-2, pp. 51–59, 2010.

[33] A. V. Berezkin and A. R. Khokhlov, "Mathematical modeling of interfacial polycondensation," *Journal of Polymer Science Part B: Polymer Physics*, vol. 44, no. 18, pp. 2698–2724, 2006.

[34] V. Freger and S. Srebnik, "Mathematical model of charge and density distributions in interfacial polymerization of thin films," *Journal of Applied Polymer Science*, vol. 88, no. 5, pp. 1162–1169, 2003.

[35] G.-Y. Chai and W. B. Krantz, "Formation and characterization of polyamide membranes via interfacial polymerization," *Journal of Membrane Science*, vol. 93, no. 2, pp. 175–192, 1994.

[36] P. S. Singh and V. K. Aswal, "Characterization of physical structure of silica nanoparticles encapsulated in polymeric structure of polyamide films," *Journal of Colloid and Interface Science*, vol. 326, no. 1, pp. 176–185, 2008.

[37] S.-Y. Kwak, S. H. Kim, and S. S. Kim, "Hybrid organic/inorganic reverse osmosis (RO) membrane for bactericidal anti-fouling. 1. Preparation and characterization of TiO_2 nanoparticle self-assembled aromatic polyamide thin-film-composite (TFC) membrane," *Environmental Science and Technology*, vol. 35, no. 11, pp. 2388–2394, 2001.

[38] H. Yan, X. Miao, J. Xu et al., "The porous structure of the fully-aromatic polyamide film in reverse osmosis membranes," *Journal of Membrane Science*, vol. 475, pp. 504–510, 2015.

[39] T. A. Saleh and V. K. Gupta, "Synthesis and characterization of alumina nano-particles polyamide membrane with enhanced flux rejection performance," *Separation and Purification Technology*, vol. 89, pp. 245–251, 2012.